

Surface-bound chemical vapour deposition of carbon nanotubes: In situ study of catalyst activation

C. Mattevi^{a,b,c,*}, S. Hofmann^d, M. Cantoro^{d,1}, A.C. Ferrari^d, J. Robertson^d,
C. Castellarin-Cudia^e, S. Dolafi^{c,e}, A. Goldoni^e, C. Cepek^b

^aDipartimento di Scienze Chimiche, University of Padova, Via Marzolo 1, I-335131 Padova, Italy

^bLaboratorio Nazionale TASC-CNR-INFN, ss 14, km 163.5, I-34012 Trieste, Italy

^cAREA Science Park, Padriciano 99, I-34012 Trieste, Italy

^dDepartment of Engineering, University of Cambridge, Cambridge CB3 0FA, UK

^eSurface Science Division, Sincrotrone Trieste SCA, ss 14, km 163.5, I-34012 Trieste, Italy

Available online 13 October 2007

Abstract

We combine in situ X-ray photoelectron spectroscopy and ex situ electron and Raman spectroscopy to study chemical interactions of SiO₂-supported Fe catalyst films during C₂H₂ exposure in the 400–600 °C temperature range. Carbon nanotubes nucleate at C₂H₂ pressures below 10⁻⁶ mbar, which allows a time-resolved recording of core level spectra. We find a rapid transition from an initial chemisorbed carbon on metallic Fe catalyst nanoparticles to a sp² graphitic carbon network. Pre-treating the Fe catalyst film by H₂ sputtering influences the initial catalyst de-wetting and increases carbon nanotube yield.

© 2007 Elsevier B.V. All rights reserved.

PACS: 81.15Gh; 61.46.Fg; 79.60.i; 78.47.+P

Keywords: Carbon nanotubes; CVD; XPS; Spectroscopy

1. Introduction

Carbon nanotubes (CNTs) have extraordinary mechanical and thermal properties, like the highest Young's modulus and highest axial thermal conductivity among any solid [1]. Moreover, single-wall nanotubes (SWNTs) have the highest current carrying capacity of any conductor, which makes them very attractive for use in future (hybrid) integrated circuits [2]. Since their discovery, much effort has been devoted to improve their quality and gain control on their characteristics by progressive development of the growth techniques. Chemical vapour deposition (CVD), being scalable and surface-bound, is one of the viable techniques to achieve full compatibility with the existing microelectronic processes [3,4]. The final aim

would be to minimize the number of defects and to achieve a better control on properties such as diameter, length, and chirality. A complete knowledge of the catalyst substrate interaction, together with the understanding of the carbon precursor gas dissociation/de-hydrogenation mechanism during CVD, is fundamental to allow for a high degree of control and synthesize a specific tubular form of carbon.

Here, we present a systematic photoemission spectroscopy investigation of the chemical interaction between the catalyst and the carbon precursor gas, before and during CNT CVD, and discuss the role of the catalyst pre-treatment. Experiments are carried out in two different UHV systems. The catalyst deposition and the CVD steps are performed in sequence, without breaking the vacuum, to avoid any contamination and/or catalyst oxidation side effects. Monitoring of the Fe 2p_{1/2}–2p_{3/2} peaks allows us to assess the mechanisms involved during a H₂ sputtering pre-treatment performed on the catalyst film. The C 1s photoemission peak, during the carbon precursor gas

*Corresponding author.

E-mail address: mattevi@tasc.infn.it (C. Mattevi).

¹Present address: IMEC vzw, Kapeldreef 75, 3001 Leuven, Belgium.

dosing, is constantly monitored to reveal details about the dynamics of the chemical changes involved during CNT nucleation/growth.

2. Experimental

Two sets of X-ray photoemission spectroscopy (XPS) experiments are performed. In situ Fe $2p$ photoemission spectra are acquired in normal emission geometry, using a conventional Mg X-ray source ($h\nu = 1253.6$ eV) with an overall energy resolution of ~ 1.2 eV. In situ time-resolved XPS spectra from the C $1s$ core level are measured in the UHV end station of the SuperESCA beamline (base pressure $< 10^{-10}$ mbar) at the ELETTRA Synchrotron, Trieste, Italy. A high flux of 400 eV photons allows core level spectra to be acquired within 15 s, with an energy resolution below 80 meV (probe size $\sim 30 \times 200 \mu\text{m}^2$). We stress that in situ, *fast* time-resolved XPS measurements can only be carried out using a high-brilliance photon source, such as a synchrotron light beam.

For all the experiments, we utilize commercial, polished n-type Si(100) substrates, topped with a 150 nm thermally grown SiO_2 film. Fe catalyst films are deposited in situ by sublimation from heated filaments (Aldrich, 99.9% purity) at a growth rate of ~ 0.6 nm/h (calibrated by XPS). Samples are clamped between two Ta contacts and heated by direct heating. Fe films are always monitored by XPS to detect the presence of any contaminant and/or silicides. For CNT growth, undiluted C_2H_2 is let into the SuperESCA chamber using a gas-doser with a micro-channel plate head, 15 mm away from the sample. This setup allows in situ measurements in gas background pressures up to 5×10^{-7} mbar. In the other chamber, C_2H_2 is let in through a 1/4 in. stainless-steel pipe, whose nozzle is 1 cm away from the sample. All samples are also characterized ex situ by scanning electron microscopy (SEM, LEO 1530VP FEGSEM) and Raman spectroscopy (Renishaw 1000 spectrometer, 633 nm laser excitation, $50 \times$ objective, maximum power on the sample $\sim 10^9$ W/m 2).

We operate in the following parameter window: ~ 0.08 – 0.6 nm Fe film thickness, 4×10^{-8} – 8×10^{-3} mbar C_2H_2 pressure and 400 – 600 °C CNT growth temperature. A typical CVD route consists of a preliminary out-gassing of the Si/SiO $_2$ substrate at 550 – 600 °C, followed by Fe deposition at room temperature, and successive ramping-up to the chosen CNT growth temperature. We also investigate the effects of additional pre-treating of the catalyst by H_2 sputtering (sputter gun, $E_{\text{ions}} = 300$ eV) prior to CNT growth.

3. Results

3.1. Role of catalyst pre-treatment

We detect an increase in CNT yield when pre-treating the Fe catalyst film (performing a H_2 sputtering) prior to growth. We detect SWNTs with the highest yield when

using ~ 0.15 – 0.6 -nm-thick Fe films, sputtered with H_2 and exposed at C_2H_2 pressures greater than 8×10^{-6} mbar, at 550 – 600 °C. Lower SWNT yields are generally observed at lower pressures ($< 10^{-7}$ mbar). At even lower pressures, and at temperatures below 550 °C, carbon nanofibres (CNFs) or even no carbon structures are detected.

Fig. 1 shows the results of a CVD run with high SWNT yield. Growth is performed by exposing an annealed (at 580 °C, 5 min) and H_2 sputtered (at 580 °C, 5 min), 0.5 -nm-thick Fe film (Si/SiO $_2$ -supported) to undiluted C_2H_2 (8×10^{-4} mbar pressure) for 5 min at 580 °C. This

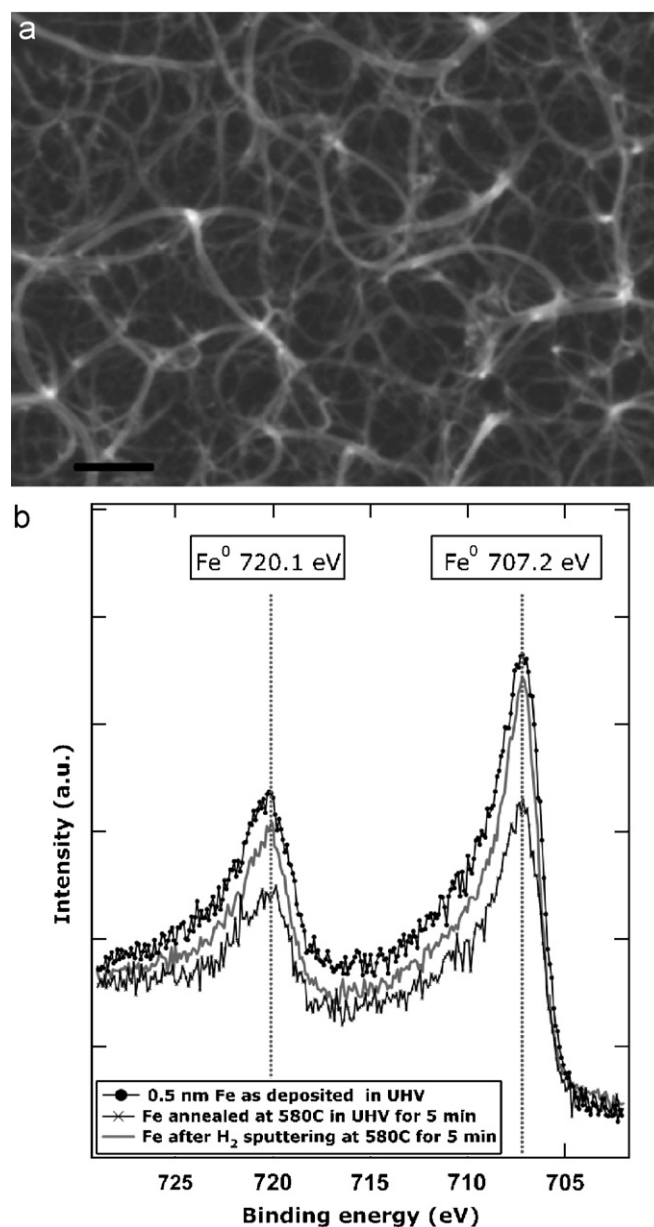


Fig. 1. (a) SEM image of SWNT bundles grown on Si/SiO $_2$ substrates by exposing an annealed (at 580 °C, 5 min) and H_2 sputtered (at 580 °C, 5 min), 0.5 -nm-thick Fe film to undiluted C_2H_2 (8×10^{-4} mbar pressure) for 5 min at 580 °C (scale bar: 100 nm). (b) Fe $2p_{1/2}$ – $2p_{3/2}$ photoemission spectra ($h\nu = 1253.6$ eV) acquired after every step of the pretreatment process described in (a). All spectra are normalized to the photon flux.

confirms our previous observation that catalyst reconstruction by weak H_2 or NH_3 plasmas (or by purely thermal annealing in gaseous atmosphere) is beneficial to the increase of the CNT yield [5–8]. AFM analysis reveals that after such a pre-treatment, the catalyst reconstructs in smaller islands with a narrower diameter distribution, if compared to an annealing stage in vacuum, without pre-treatment [5–8].

The substrate used to grow the CNT sample in Fig. 1 was characterized by in situ XPS with the intent of monitoring any chemical changes of the Fe– SiO_2 interaction after each of the individual CVD steps prior to growth (catalyst deposition, annealing, H_2 sputtering). The evolution of the Fe $2p$ spectra is shown in Fig. 1(b). The binding energy of the $2p_{3/2}$ line of the as-deposited Fe (707.2 eV) corresponds to its metallic chemical state [9]. No peaks attributable to contaminants or Fe silicides are detected. After Fe annealing at 580 °C, no significant lineshape changes are observed. However, the absolute intensity of the Fe $2p_{3/2}$ peak decreases by 35% (Fig. 1(b)). This is caused by the de-wetting of the Fe film on the SiO_2 substrate upon annealing [6,7,10], the islands diameter distribution depending on the initial film thickness and annealing temperature [11,12]. For our experiments, it is reasonable to assume that the Fe film is characterized by larger islands before being subjected to the H_2 sputtering [4,7,8,13]. A confirmation of the “morphological” effect of the H_2 sputtering is suggested by the analysis of the Fe $2p$ photoemission spectrum (Fig. 1(b)). We find the Fe $2p$ peak intensity to increase after H_2 sputtering with respect to the corresponding Fe $2p$ signal measured after UHV annealing. This increase indicates that Fe covers more substrate surface after H_2 sputtering than after an annealing stage in UHV, implying that islands diameters and heights are larger after UHV annealing than after H_2 sputtering.

No Fe $2p$ lineshape changes are observed throughout all the steps of catalyst preparation, as also confirmed by UV photoemission measurements. We can therefore rule out any chemical effect of H_2 sputtering on the catalyst. H_2 sputtering could create Fe– SiO_2 bonds [14], preventing Fe sintering during sample heating. Partial burial of Fe clusters into the underlying SiO_2 layer could induce a chemical reduction of the latter accompanied by concurrent Fe oxidation, as observed in the case of Fe deposited on native SiO_2 [14]. However, our XPS results (Fig. 1(b)) indicate that Fe remains metallic. Therefore, the formation of strong Fe– SiO_2 bonds can be ruled out. We cannot exclude a chemical effect of H ions on the catalyst involving weak chemical bonds, e.g. H chemisorption [15]. Chemisorbed species such as H can significantly modify the catalyst surface energies [16] leading to temperature- and pressure-dependent surface reconstruction, thus altering the interaction with C_2H_2 . Hydrogen penetration into subsurface layers can loosen the catalyst surface [16] and may give higher carbon diffusivities during SWNT nucleation.

Note that catalyst films of equivalent thickness on different supports (e.g. SiO_2 , Al_2O_3) can give different results [5,17,18]. In addition, recent calculations modelled the behaviour of free and Al_2O_3 -supported Fe nanoparticles suggesting different implications for SWNT growth [19].

3.2. Chemical changes during CNT nucleation

The Fe– C_2H_2 interaction during the CNT growth stage is investigated in the SuperESCA chamber through in situ monitoring of the C $1s$ peak time evolution [20]. No C $1s$ peak is detected on samples where the Fe catalyst is not present, thus ruling out any possible interaction between C_2H_2 and the SiO_2 surface in our experimental conditions.

Fig. 2 shows the results of CNT CVD performed on to H_2 sputtered Fe films in the same experimental conditions as for Fig. 1, but at lower C_2H_2 pressure (2×10^{-7} mbar). Fig. 2(b) shows the time-resolved evolution of the C $1s$ peak. Its dynamics can be described as follows: as soon as C_2H_2 is let into the chamber, a peak at 282.6 eV appears, indicating that C is chemisorbed on the Fe catalyst [21,22]. After 90 s incubation, another peak at 283.2 eV appears, persisting for 30 s. We attribute this peak to the formation of carbidic C [21,23]. The formation of a sp^2 , graphitic C network is detected by the appearance of another peak at 284.5 eV (corresponding to the typical C $1s$ binding energy of the C–C bond) [21,24]. The intensity of the latter peak increases very rapidly: after 15 s, the chemisorbed C and carbidic C peaks drastically reduce. The graphitic peak saturates after 150 s, suggesting a termination of CNT growth, and dominates over the chemisorbed C and carbidic C peaks. A SEM picture of the as-grown sample is presented in Fig. 2(a), showing the presence of laterally extended, sparse CNTs.

Raman spectroscopy is a fast and non-destructive method for characterization of carbon materials [25]. In the case of SWNTs, important information such as diameter, orientation, metallic or semiconducting character and chirality, can be obtained from a Raman spectrum [26–30]. Fig. 3(a) shows a Raman spectrum (633 nm) of the sample shown in Fig. 2(a). We observe a structured G peak at $\sim 1600\text{ cm}^{-1}$, typical of nanotubes [26–30], and the D peak at $\sim 1300\text{ cm}^{-1}$, indicative of defects and disordered graphitic material [31]. The presence of well-defined radial breathing modes (RBMs) in the low frequency range (inset in Fig. 3), together with the shape of the G peak, is the typical signature of SWNTs [26,27]. SWNT diameters (corresponding to the RBMs observed) can be calculated using $d = C_1/(\omega_{RBM} - C_2)$, with $C_1 = 214.4\text{ nm/cm}$ and $C_2 = 18.7\text{ cm}^{-1}$ [28], resulting in a 0.8–1.3 nm diameter distribution. Due to the cut-off of our notch filter, we cannot detect SWNT diameters $> 2\text{ nm}$.

The C $1s$ peak time evolution (Fig. 2(b)) shows an increase of binding energy throughout the continuous transition from a chemisorbed C form (282.6 eV) [21,22] to carbidic C (283.2 eV) [21,23], and ultimately to a

re-organization of the C atoms in a sp^2 network (284.5 eV, CNT growth) [21,24]. Our data indicate that the chemisorbed C state persists up to 25 at% C concentration. At

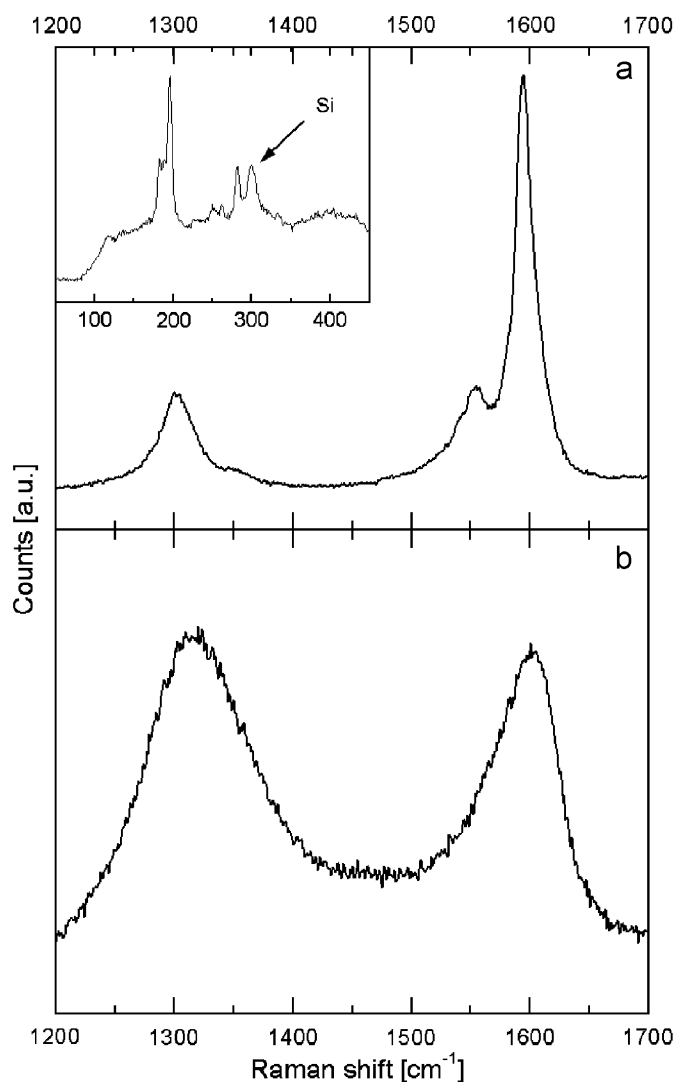
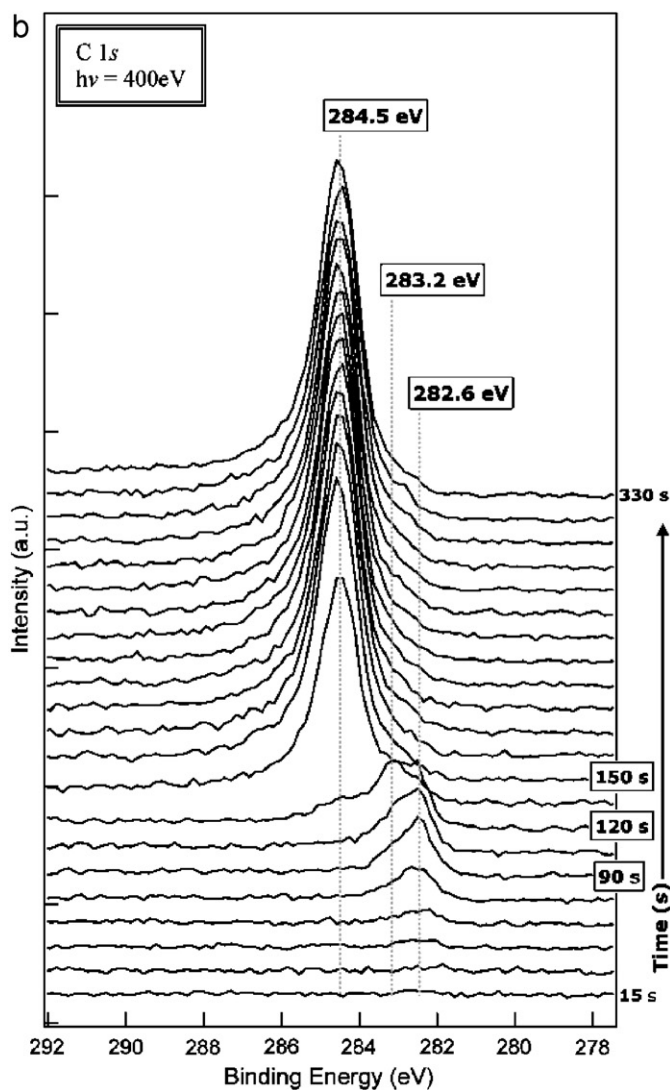
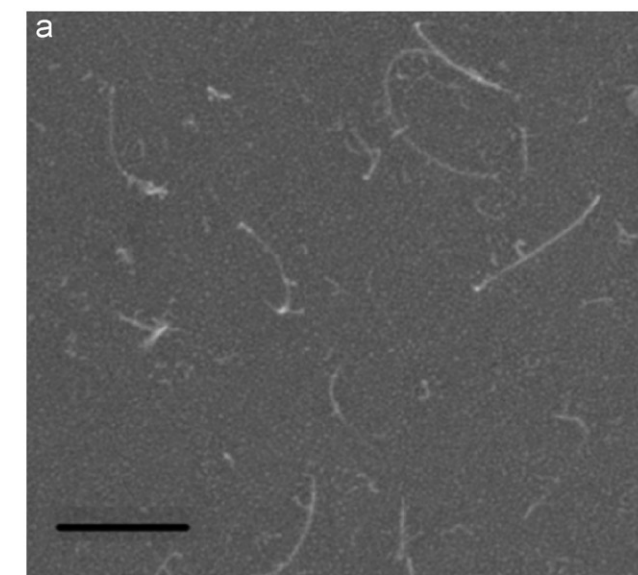


Fig. 3. Raman spectra of two CNT samples grown in the SuperESCA chamber. Sample (a) is that depicted in Fig. 2(a). Sample (b) is grown by exposing a H_2 sputtered (5 min), 0.4-nm-thick Fe film (on Si/SiO₂ support) to undiluted C_2H_2 at 4×10^{-8} mbar for 5 min at 600 °C.

higher concentrations, the C–Fe bond changes, and the carbidic C signature at 283.2 eV appears.

In literature, a binding energy of 282.6 eV, measured by XPS on the surface of Fe single crystals annealed at high temperatures, was attributed to chemisorbed C [21,22]. In Ref. [22], chemisorbed C of sub-monolayer thickness was measured after sample heating up to temperatures in the 377–577 °C range. In Ref. [21], the Fe sample was heated at temperatures between 450 and 700 °C, obtaining again sub-monolayer-thick chemisorbed C or graphitic C on the metal surface as separate phases, reversibly transformed into

Fig. 2. (a) SEM image of SWNT bundles grown on Si/SiO₂ substrates by exposing a H_2 sputtered (at 580 °C, 1 h), 0.5-nm-thick Fe film to undiluted C_2H_2 (2×10^{-7} mbar pressure) for 5 min at 580 °C (scale bar: 200 nm). (b) Time-resolved evolution of the C 1s photoemission spectrum during CVD of the sample described in (a). The spectra (normalized to the photon flux) are recorded every 15 s. The dotted vertical lines indicate the binding energies of the different carbon species formed during the CVD process.

each other under specific annealing conditions. We thus use Ref. [21] to define the reference binding energies for chemisorbed C and graphitic C, since they are characterized by XPS a system similar to ours (carbon bonded to Fe).

We observe a similar time evolution of the C 1s peak when using slightly different CVD conditions for CNT growth. Fig. 3(b) shows the Raman spectrum (633 nm) of sample grown by exposing a H₂ sputtered (5 min), 0.4-nm-thick Fe film to undiluted C₂H₂ (4×10^{-8} mbar pressure) for 5 min at 600 °C. The spectrum is characterized by very broad D and G peaks, typical of disordered carbons and non-highly crystalline tubular structures such as CNFs [31]. However, in situ monitoring of the C 1s peak time evolution (in the SuperESCA chamber) reveals a dynamics very similar to that described for the SWNT sample in Fig. 2. We attribute the differences between the samples whose Raman is in Fig. 3(a) and (b) to the concurrently effects of the changes in H₂ sputtering time duration prior to growth and to the different C₂H₂ pressure.

We are currently investigating the effects of hydrocarbon gas dosing, and preliminary results show that the tendency to form defective tubular carbon structures depends on the rate of carbon feeding: fast hydrocarbon gas pressure gradients can result in CNT growth at low pressures (2×10^{-7} mbar), while higher pressures are less sensitive to such gradients [32].

4. Conclusions

We presented an investigation of CNT growth by CVD in UHV conditions, by exposing in situ deposited Fe films on Si/SiO₂ to undiluted C₂H₂ at pressures in the 4×10^{-8} – 8×10^{-3} mbar range. Continuous monitoring of the relevant photoemission peaks allow us to conclude that a catalyst pre-treatment (H₂ sputtering) during CNT growth can significantly improve the CNT yield. No Fe 2p lineshape changes were observed throughout all the steps of catalyst preparation, hence we rule out the formation of strong Fe–SiO₂ bonds. Chemical changes of the Fe–C₂H₂ interaction occurring in the early stages of CNT nucleation/growth were monitored by time-resolved photoemission. We observed that a rapid transition from an initial chemisorbed C on the metallic Fe catalyst to a sp² C network occurs, through the formation of an intermediate carbidic stage.

Acknowledgements

C.C. and C.M. acknowledge the FIRB project “Carbon-based nanostructures and microstructures”. S.H. and A.C.F. acknowledge funding from the Royal Society. S.H. acknowledges Peterhouse, Cambridge, and A.C.F. acknowledges the Leverhulme Trust.

References

- [1] M. Terrones, *Annu. Rev. Mater. Res.* 33 (2003) 419.
- [2] Ph. Avouris, J. Chen, *Mater. Today* 9 (2006) 46.
- [3] H. Dai, *Acc. Chem. Res.* 35 (2002) 1035.
- [4] R. Vajtai, B.Q. Wei, P.M. Ajayan, *Philos. Trans. R. Soc. Lond. A* 362 (2004) 2143.
- [5] M. Cantoro, S. Hofmann, S. Pisana, V. Scardaci, A. Parvez, C. Ducati, A.C. Ferrari, A.M. Blackburn, K.Y. Wang, J. Robertson, *Nano Lett.* 6 (2006) 1107.
- [6] S. Pisana, M. Cantoro, A. Parvez, S. Hofmann, A.C. Ferrari, J. Robertson, *Physica E* 37 (2006) 1.
- [7] M. Cantoro, S. Hofmann, S. Pisana, C. Ducati, A. Parvez, A.C. Ferrari, J. Robertson, *Diamond Relat. Mater.* 15 (2006) 1029.
- [8] S. Hofmann, M. Cantoro, B. Kleinsorge, C. Casiraghi, A. Parvez, C. Ducati, J. Robertson, *J. Appl. Phys.* 98 (2005) 34308.
- [9] G. Panzner, B. Egert, *Surf. Sci.* 144 (1984) 651.
- [10] R. Pretorius, J.M. Harris, M.-A. Nicolet, *Solid State Electron.* 21 (1978) 667.
- [11] J.F. Colomer, C. Stephan, S. Lefrant, *Chem. Phys. Lett.* 317 (2000) 83.
- [12] Y.Y. Wei, G. Eres, V.I. Merkulov, D.H. Lowndes, *Appl. Phys. Lett.* 78 (2001) 1394.
- [13] S. Hofmann, C. Ducati, B. Kleinsorge, J. Robertson, *Appl. Phys. Lett.* 83 (2003) 135.
- [14] M.G. Garnier, T. de los Arcos, J. Boudaden, P. Oelhafen, *Surf. Sci.* 536 (2003) 138.
- [15] W.F. Egelhoff, D.A. Steigerwald, *J. Vac. Sci. Technol. A* 7 (1989) 2167.
- [16] Z. Paal, P.G. Menon, *Hydrogen Effects in Catalysis*, Dekker, New York, 1988.
- [17] R. Seidel, G.S. Duesberg, E. Unger, A.P. Graham, M. Liebau, F. Kreupl, *J. Phys. Chem. B* 108 (2004) 1888.
- [18] T. de los Arcos, M.G. Garnier, J.W. Seo, P. Oelhafen, V. Thommen, D. Mathys, *J. Phys. Chem. B* 108 (2004) 7728.
- [19] A. Jiang, N. Awasthi, A.N. Kolmogorov, W. Setyawan, A. Börjesson, K. Bolton, A.R. Harutyunyan, S. Curtarolo, *Phys. Rev. B* 75 (2007) 205426.
- [20] S. Hofmann, R. Sharma, C. Ducati, G. Du, C. Mattevi, C. Cepek, M. Cantoro, S. Pisana, A. Parvez, F. Cervantes-Sodi, A.C. Ferrari, R. Dunin-Borkowski, S. Lizzit, L. Petaccia, A. Goldoni, J. Robertson, *Nano Lett.* 7 (2007) 602.
- [21] G. Panzner, W. Diekmann, *Surf. Sci.* 160 (1985) 253.
- [22] G. Panaccione, J. Fujii, I. Vobornik, G. Trimarchi, N. Binggeli, A. Goldoni, R. Larciprete, G. Rossi, *Phys. Rev. B* 73 (2006) 35431.
- [23] A. Wiltner, C. Linsmeier, *Phys. Status Solidi A* 201 (2004) 881.
- [24] J.C. Lascovich, R. Giorgi, S. Scaglione, *Appl. Surf. Sci.* 47 (1991) 17.
- [25] A.C. Ferrari, J. Robertson, *Philos. Trans. R. Soc. Lond. A* 362 (2004) 2477.
- [26] A. Jorio, A.G. Souza, G. Dresselhaus, M.S. Dresselhaus, A.K. Swan, M.S. Unlu, B.B. Goldberg, M.A. Pimenta, J.H. Hafner, C.M. Lieber, R. Saito, *Phys. Rev. B* 65 (2002) 155412.
- [27] J. Maultzsch, S. Reich, U. Schlecht, C. Thomsen, *Phys. Rev. Lett.* 91 (2003) 087402.
- [28] H. Telg, J. Maultzsch, S. Reich, F. Hennrich, C. Thomsen, *Phys. Rev. Lett.* 93 (2004) 177401.
- [29] M. Lazzeri, S. Piscanec, F. Mauri, A.C. Ferrari, J. Robertson, *Phys. Rev. B* 73 (2006) 155426.
- [30] S. Piscanec, M. Lazzeri, J. Robertson, A.C. Ferrari, F. Mauri, *Phys. Rev. B* 75 (2007) 035427.
- [31] A.C. Ferrari, J. Robertson, *Phys. Rev. B* 61 (2000) 14095.
- [32] C. Mattevi, et al., in preparation.